Supporting Information

Near-Infrared Photoactivatable Nitric Oxide Donors with Integrated Photoacoustic Monitoring

Effie Y. Zhou,[†&] Hailey J Knox,[†&] Christopher J. Reinhardt,[†] Gina Partipilo,[†] Mark J. Nilges[‡] and Jefferson Chan[†*]

[†]Department of Chemistry and Beckman Institute for Advanced Science and Technology, University of Illinois at Urbana-Champaign, 600 S. Mathews Ave, Urbana, Illinois 61801 (USA)

[‡]The Illinois EPR Research Center, University of Illinois at Urbana-Champaign, Urbana, IL, 61801 (USA)

[&]These authors contributed equally

Correspondence should be addressed to J.C. (jeffchan@illinois.edu).

1. Materials ……. S2
2. Instrumentation …… S2
3. Data Processing……. S3
4. Tissue phantom preparation ……..S3
5. pH Stability ……S3
6. Approximate quantification of NO photorelease ……. S3
7. Mass spectrometry validation of PA turnover …… S4
8. Cell culture information ……... S4
9. Cytotoxicity assay ……..……S4
10. Proliferation assay S5
10. *In vivo* PA spectra ……..... S5
11. TUNEL IHC assay S5
11. Supplementary figures …… S6
14. NMR spectra……..S14
15. References ……S22

Materials. Boric acid, dichloromethane, and triethylamine were purchased from Acros Organics. Nitromethane was purchased from Alfa Aesar. Ammonium acetate was purchased from Amersco. NADPH tetrasodium salt was purchased from CalBioChem. Methylamine hexamethylene methylamine NONOate (MAHMA-NONOate) was purchased from Cayman Chemicals. All deuterated solvents were purchased from Cambridge Isotope Laboratories. Tris(3-hydroxypropyltriazolyl-methyl)amine was purchased from Click Chemistry Tools. *N*-(dithiocarbamoyl)-N-methyl-D-glucamine (MGD) was purchased from Enzo Life Sciences. Acetic acid, anhydrous ethanol (Decon Lab), chloroform, copper sulfate pentahydrate, Cremophor EL (CrEL) (Fluka), cryomolds (Andwin Scientific Tissue Tek), ethyl acetate, matrigel (Corning, phenol red-free), *n*-butanol, phosphate buffered saline (PBS) (Corning), *o*-phosphoric acid, OCT compound (Fisher Healthcare Tissue Plus), potassium phosphate dibasic, potassium phosphate monobasic, propidium iodide, sodium bicarbonate, sodium carbonate, and sodium chloride were purchased from Fisher Scientific. Agarose LE (Molecular Biology Grade) was purchased from Gold Biotechnology. Silica and neutral alumina were purchased from Macherey-Nagel. Anhydrous methanol and isopropanol were purchased from Macron Fine Chemicals. Fluorinated ethylene propylene (FEP) tubing (wall thickness 0.01", inner diameters 0.08" and 0.12") was purchased from McMaster-Carr. 4'-aminoacetophenone, di-*tert*-butyl dicarbonate, methyl iodide, potassium hydroxide, and sodium sulfate (anhydrous) were purchased from Oakwood Chemicals. 1,4-Dioxane, anhydrous dichloromethane, anhydrous dimethysulfoxide, anhydrous tetrahydrofuran, benzaldehyde, boron trifluoride diethyl etherate, celite 545, copper(II) chloride, HEPES, hexanes, iron(II) sulfate heptahydrate, iron(III) chloride (anhydrous), sodium hydride (60 % dispersion in mineral oil), sodium ascorbate, sodium nitrite, tetrakis(acetonitrile) copper(I) hexafluorophosphate, trifluoroacetic acid, rat liver microsomes, human plasma, and Wilmad® quartz (cfq) EPR tubes (OD 4.0 mm, L 250 mm) were purchased from Sigma Aldrich. Hoechst 33342 stain and Shandon™ Polysine slides were purchased from Thermo Fisher Scientific. Capillary tube holding tray with wax plates (24 place) and micro haematocrit tubes (soda lime glass, blue tip, plain) were purchased from Thomas Scientific.

Instrumentation. Absorbance spectra were acquired with an Agilent Cary 60 UV-Vis spectrophotometer. EPR data was collected with a Varian E-line 12" Century Series X-band CW EPR (VarianXBand). Cytotoxicity assays were conducted using an EVOS FL epifluorescence

microscope equipped with an RFP filter cube and a DAPI filter cube. A Nexus 128 Photoacoustic Tomographer (Endra Life Sciences) was used for irradiations and acquiring photoacoustic data and images.

Data processing. PA images were analysed using Horos software (v 3.0). Thick slab processing was used to visualize accumulated signal over 8.0 mm *in vivo* and 4.0 mm *in vitro*. Mean PA signal was determined within ROIs of equal area, and ratiometric turn-on response was calculated using the fold change in the $\lambda_{red}/\lambda_{blue}$ signal ratio at each time point. Statistical analyses were performed using GraphPad Prism (version 6.0c). All data were analyzed using Student's t-tests, and are presented as mean ± SD.

Tissue phantom preparation. Tissue phantoms were prepared by suspending agarose LE in a solution of 2% milk (2 mL) and deionized water (78 mL). The suspension was heated in a microwave until a viscous, translucent gel was produced. The hot gel was poured into a custom Teflon mold containing two copper tubes and cooled at – 4 °C for at least 2 hours. After cooling, the copper tubes were removed and the gel was removed from the mold, yielding a tissue phantom with two parallel channels for the placement of FEP tubes containing sample solutions.

pH Stability. Britton-Robinson buffers prepared as described in the literature.[1] Briefly, acetic acid, phosphoric acid, and boric acid were mixed to a concentration of 0.04 M each, and the pH of this solution was adjusted by addition of 0.2M NaOH. The resulting solutions were then diluted (1:1) with either ethanol, or water followed by addition of 0.1% (v/v) CrEL, and the pH values were then verified. pH studies were conducted by dissolving photoNOD-1 or rNOD-1 in ethanolic buffer (and incubating at 37 °C for > 10 min to solubilize) and photoNOD-2 or rNOD-2 in buffer with CrEL and acquiring absorbance spectra (400 nm to 900 nm). Relative stability was plotted by determining the ratio of absorbances at λ_{red} to λ_{blue} at each pH (Figure S9).

Approximate quantification of NO photorelease. The NO release in organic solvent was approximated from the absorbance spectra of the irradiated photoNOD samples (as described in the main text, *in vitro* irradiation) (Figure S1). Microsoft Office 15 Solver Add-in was utilized to determine the weighted contribution of photoNOD and rNOD to the post-irradiation spectra. The

molar extinction coefficient of rNOD was used to calculate the concentration. This approximation assumes a stoichiometric relationship between the amount of NO release and rNOD formation due to the finding that rNOD does not photobleach under the conditions of the experiment.

Mass spectrometry validation of PA turnover. A solution of photoNOD-1 or photoNOD-2 (200 μL, 10 μM) in chloroform was prepared and pipetted into PCR tubes. The sample was then inserted into a phantom (prepared as described above) and irradiated at λ_{blue} using the Step and Shoot mode with 120 angles and 39 pulses per angle (5 minutes of continuous irradiation). The product of irradiation was determined using LCMS and compared to a synthetic standard (Figure S2-4)

Cell culture. HEK 293T cells (ATCC) were cultured in Dulbecco's Modified Eagle's Medium, (DMEM, Corning) supplemented with 4.55% glucose, 6 mM L-glutamine, 1 mM sodium pyruvate, 10 % fetal bovine serum (FBS, Sigma Aldrich), and 1 % penicillin/streptomycin (Corning). 4T1 cells (ATCC) were cultured in RPMI 1640 Medium supplemented with 10% FBS and 1% penicillin/streptomycin. Cells were incubated at 37 °C with 5 % CO_2. Experiments were performed in 96-well plates (Nunclon Delta Surface, Thermo Scientific).

Cytotoxicity assay. A 96-well plate was seeded with HEK 293T cells (160 μL of 7.5×10^4 cells/mL). Cells were incubated for 12 h at 37 °C (50-60% confluent). Meanwhile, photoNOD-1 and -2 and rNOD-1 and -2 were dissolved in DMSO (2.7 mM) and diluted 1/10 in media to 270 μM. 20 μL of these solutions were added per well (final concentration 30 μM). The plate was incubated at 37 °C for 24 h. Propidium iodide (10 uL of 0.5 mg/mL) and Hoechst 33342 (10 μL of 0.1 mg/mL) were added to each well, and the plate was incubated at 37 °C for 15 minutes. Hoechst-stained cells were counted using a DAPI filter cube. Propidium iodide-stained cells were counted using an RFP filter cube. Percent viability was calculated by dividing the number of cells not stained by propidium iodide by the total number of Hoechst-stained cells. Assays involving 4T1 cells were seeded at 8.8×10^4 cells/mL. photoNOD-1 and rNOD-1 were dissolved in DMF at concentrations of 2.7 mM, 5.4 mM, 13.5 mM, and 27 mM and diluted 1/10 in media. Experiments were completed as described above for HEK 293T cells.

Proliferation assay. A 96-well plate was seeded with 4T1 cells (200 μL of 1.7×10^4 cells/mL). Cells were incubated for 2-3 days at 37 °C (50-60% confluent). Media was removed from the wells and replaced with 100 μL fresh media. Meanwhile, stock solutions of DEA NONOate (0, 4, 10, and 40 mM in DMSO) were prepared in degassed DMSO, then diluted 1/100 in media (0, 40, 100, and 400 μM in media). To each well was rapidly added 100 μL of the NONOate solutions (final concentrations of 0, 20, 50, and 200 μM in well). The plate was incubated at 37 °C for 12 h. The media was then aspirated. A solution of MTT (5 mg/mL in PBS) was diluted 1/20 in serum-free media, and 200 μL was added to each well. The plate was then incubated for 2 h at 37 °C. Media was aspirated and replaced with 100 μL DMSO. Proliferation was then assayed by comparing the absorbance of each well to the absorbance of the vehicle control wells at 555 nm.

***In vivo* PA spectra.** photoNOD-1, photoNOD-2, rNOD-1 and rNOD-2 (25 μL, 30 μM in sterile saline containing 2% DMSO) were each injected into the flank of a BALB/c mouse. PA images were acquired at wavelengths every 10 nm from 680 to 900 nm and the mean PA signal in regions of interest (ROIs) of equal area were plotted as a function of wavelength. Images were acquired using continuous rotation mode (6 second rotation time). Based on these PA spectra (Figure 4a and d), 710 nm ($\lambda_{PAblue)}$ and 780 nm (λ_{PAred}) were identified as optimal wavelengths for imaging photoNOD-1 and rNOD-1, respectively, while 700 nm (λ_{PAblue}) and 830 nm (λ_{PAred}) were identified as optimal wavelengths for imaging photoNOD-2 and rNOD-2, respectively.

TUNEL IHC assay. A mouse bearing tumors on both the right and left flanks was treated with photoNOD-1 (1.2 mg/kg in 150 μL sterile saline containing 20% DMSO) via retroorbital injection. Four hours following administration, the left tumor was irradiated for 5 minutes using 700 nm light (step-and-shoot mode, 120 angles, 39 pulses per angle). Fifteen minutes following irradiation, the mouse was sacrificed and tumors were excised and frozen fresh in OCT compound. Tumors were then cryosectioned using a Leica CM3050S cryostat at -22 °C. Staining was performed using an Abcam *In situ* Apoptosis Detection Kit (ab206386) according to the manufacturer's instructions and slides were imaged using a NanoZoomer Digital Pathology System (Hamamatsu Photonics).

Supplementary Figures and Tables

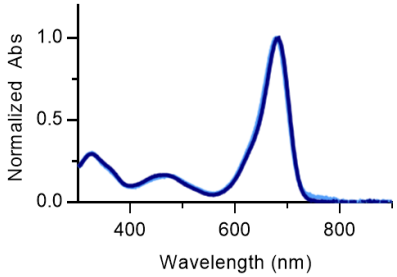

Figure S1. Absorbance spectra of photoNOD-1 (dark blue) and photoNOD-2 (light blue) in chloroform spanning the range of 300 nm to 900 nm.

Table S1. Extinction coefficients for photoNOD-1, rNOD-1, photoNOD-2, and rNOD-2 in chloroform.

Compound	λ_{max} (nm)	ε ($M^{-1}cm^{-1}$)
photoNOD-1	681	55,900
rNOD-1	733	63,400
photoNOD-2	678	44,800
rNOD-2	745	34,800

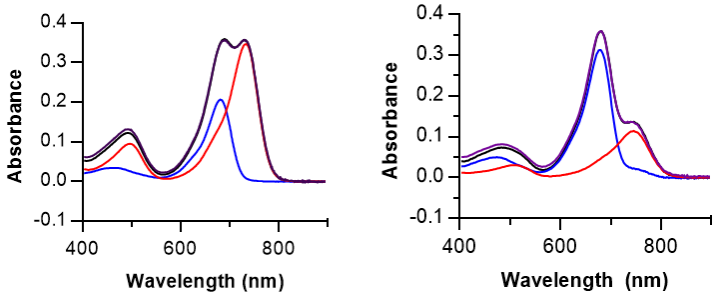

Figure S2. Representative quantification of NO release after irradiation of photoNOD-1 (left) and photoNOD-2 (right) (10 μM) in chloroform. A linear combination of the spectra of pure rNOD (red) and photoNOD (blue) yielded a calculated spectrum (black) that matched the spectrum of irradiated photoNOD (purple). The concentration of rNOD was calculated using the intensity at λ_{abs} of the red line with the extinction coefficient of rNOD in chloroform.

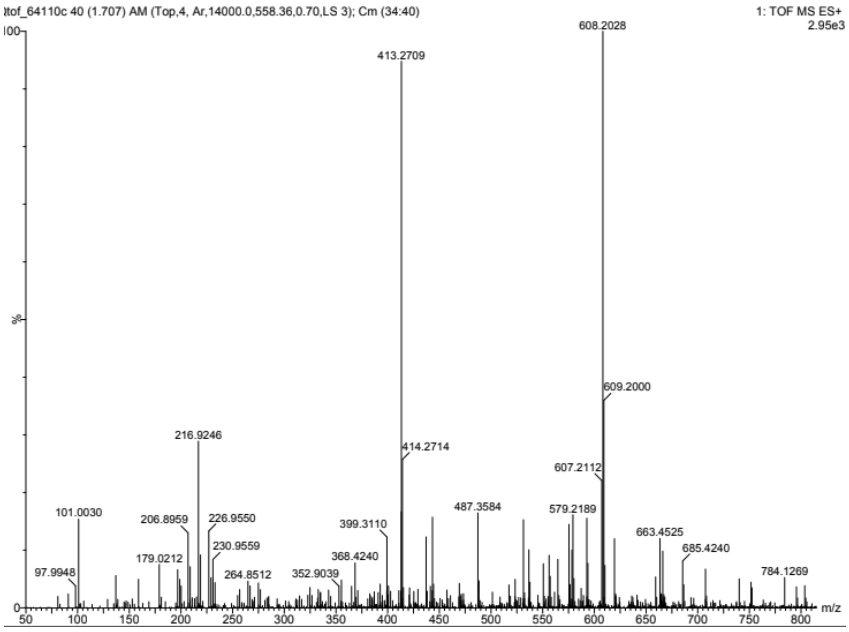

Figure S3. HRMS of photoNOD-1. [M+Na^+] 608.2040, found 608.2028.

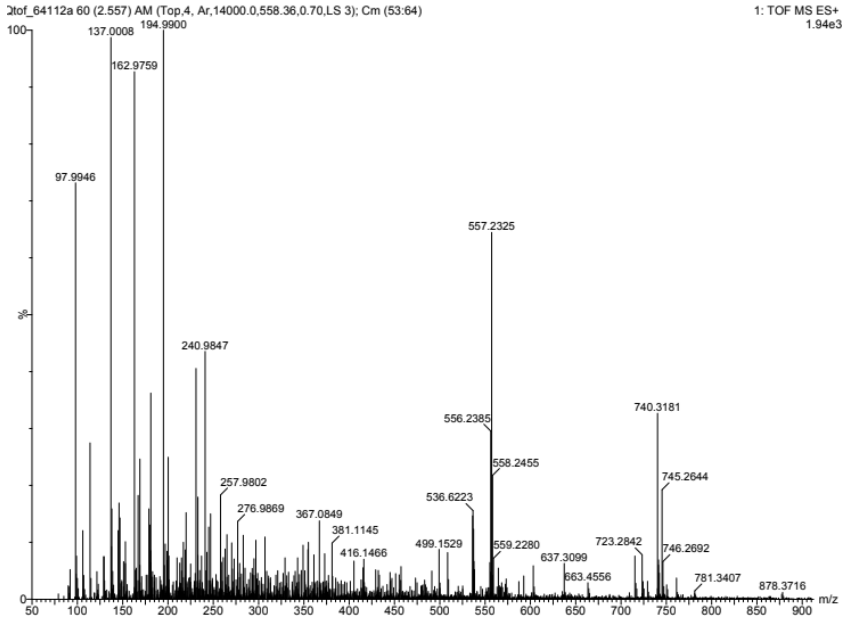

Figure S4. HRMS of rNOD-1. [M+H^+] 557.2319, found 557.2325.

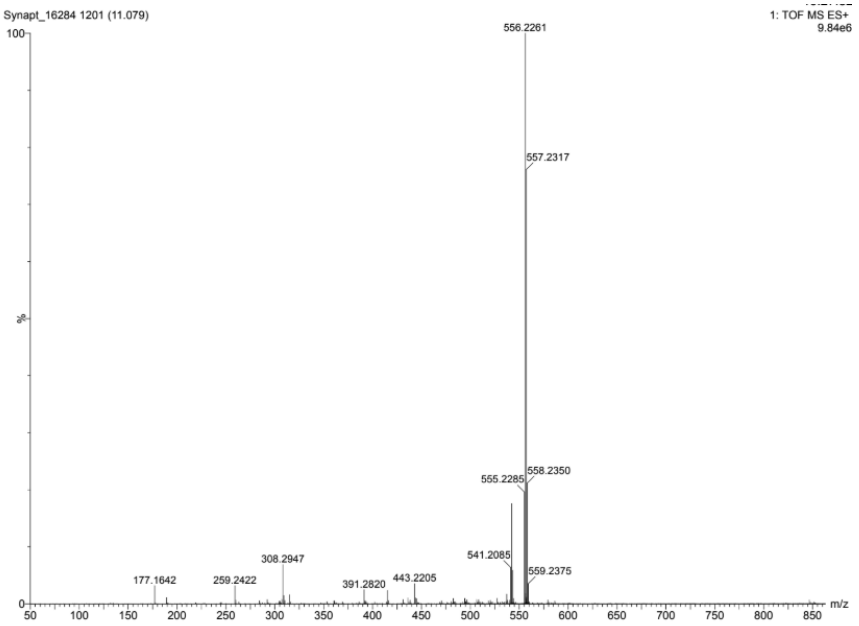

Figure S5. HRMS of photoNOD-1 after 5 min irradiation in chloroform. Found 557.2317.

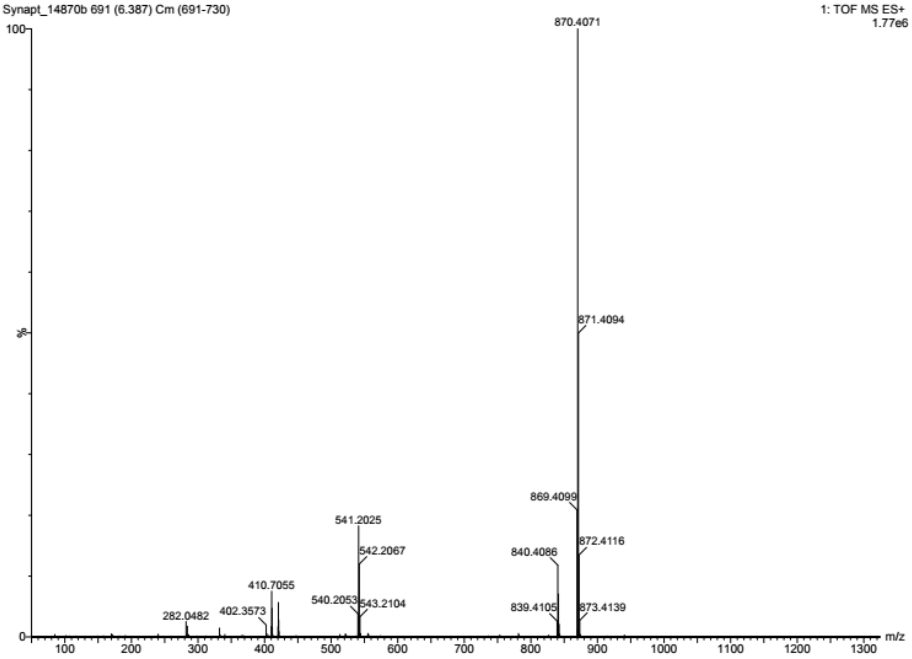

Figure S6. HRMS of photoNOD-2. [M^+] 870.4069, found 870.4071.

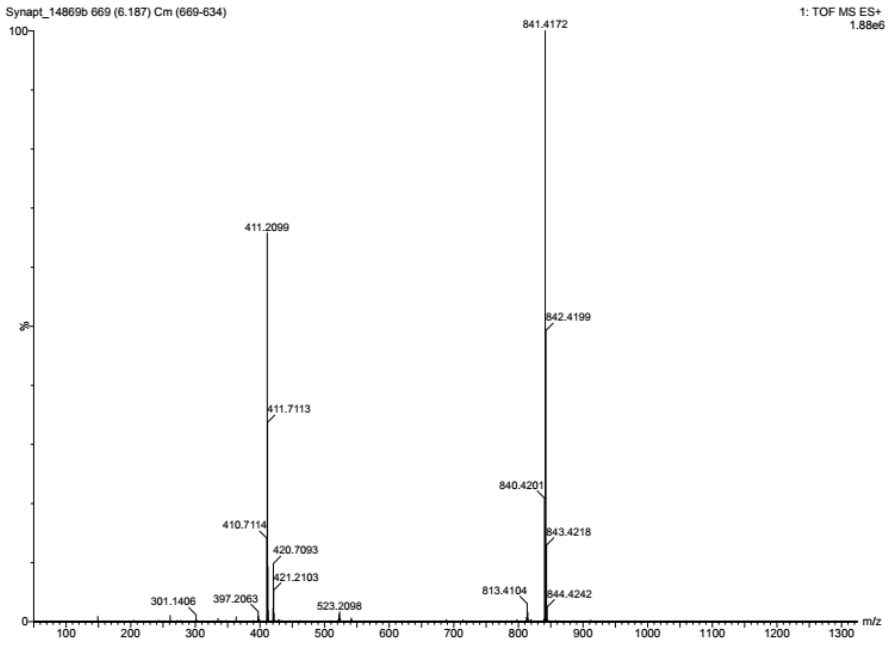

Figure S7. HRMS of rNOD-2. [M+] 841.4167, found 841.4172.

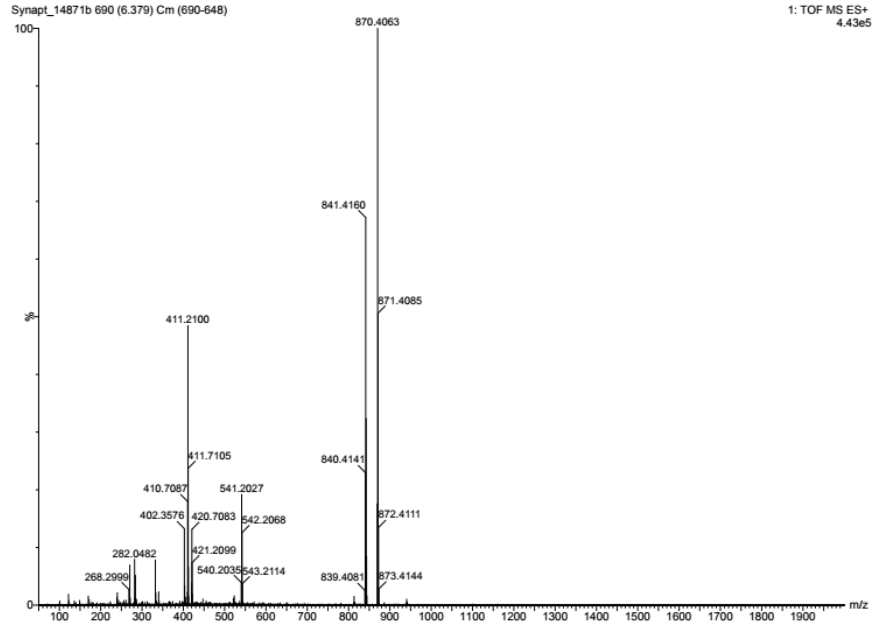

Figure S8. HRMS of photoNOD-2 after 5 min irradiation in chloroform. Found: 841.4160, 870.4063.

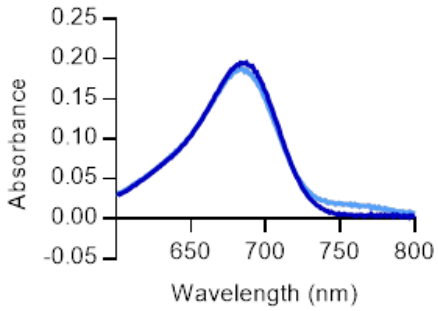

Figure S9. Absorbance spectra of photoNOD-1 (dark blue) and photoNOD-2 (light blue) in water with 50% DMF. λ_{blue} was 687 nm for photoNOD-1 and 684 nm for photoNOD-2; this enabled selection of 690 nm and 680 nm for the irradiations in the EPR experiment, respectively.

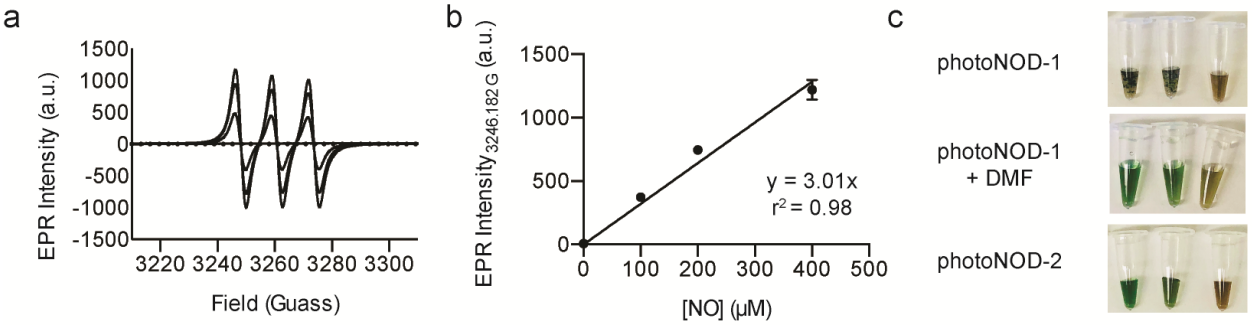

Figure S10. a) EPR spectra of spin-trapped NO released from MAHMA-NONOate (50, 100, and 200 μM). b) Calibration curve correlating EPR intensity (peak height) to concentration of NO, assuming 2 mol of NO release per mol of MAHMA-NONOate. c) Photographs of photoNOD-1 and -2 EPR samples, transferred to Eppendorf tubes after the irradiation-based experiments (left, 0 min irradiation; middle, 5 min irradiation; right, 40 min irradiation). Due to low solubility in the reaction conditions, photoNOD-1 was also shown with a 1:1 dilution in DMF.

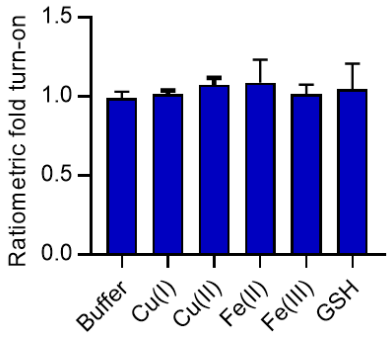

Figure S11. Ratiometric fold turn-on of photoNOD-1 upon exposure to redox-active metals (20 μM) and glutathione (1 mM) in the presence of buffer without cosolvent or surfactant. Data represented as mean ± SD (n = 3).

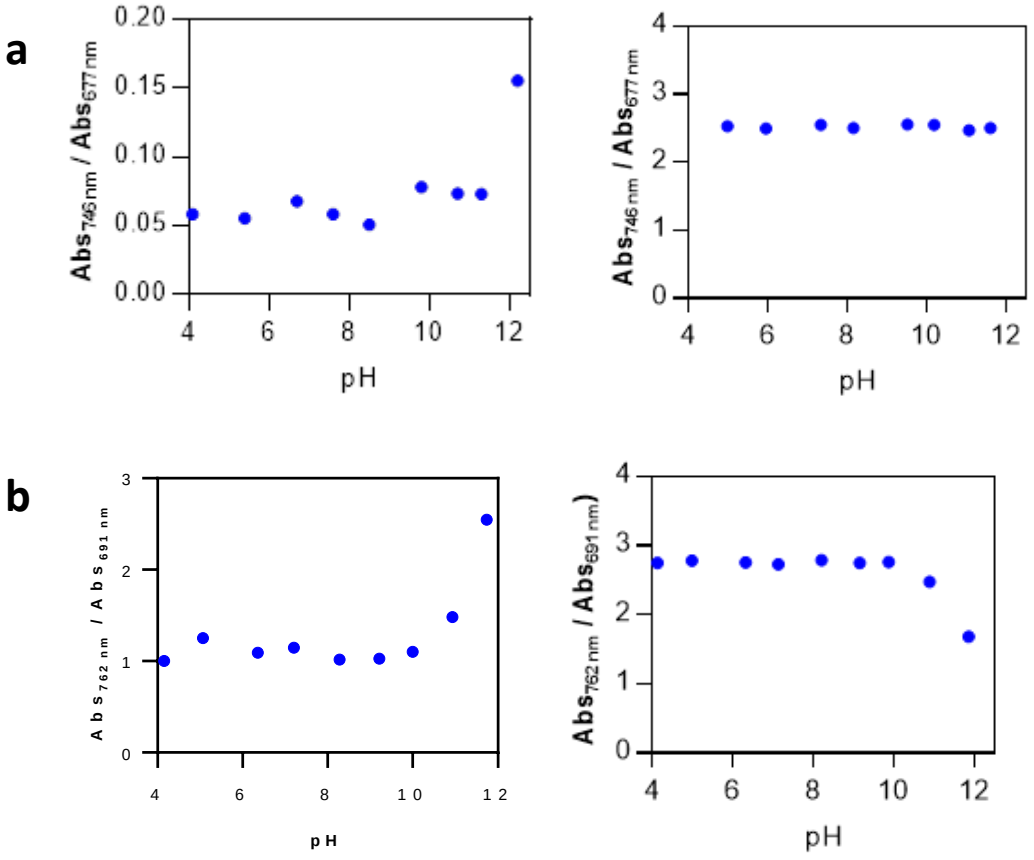

Figure S12. a) photoNOD-1 (5 μM, left; pH 4.1, 5.4, 6.7, 7.6, 8.5, 9.8, 10.7, 11.3, 12.2) and rNOD-1 (5 μM, right; pH 3.59, 4.99, 5.96, 7.34, 8.16, 9.52, 10.19, 11.07, 11.6), in Britton-Robinson buffer with 50% EtOH. b) photoNOD-2 (10 μM, left; pH 4.2, 5.1, 6.4, 7.2, 8.3, 9.2, 10. 0, 10.9,

11.7) and rNOD-2 (5 μM, right; pH 4.13, 4.99, 6.32, 7.13, 8.20, 9.15, 9.87, 10.89, 11.85) stability in Britton-Robinson buffer with 0.1% CrEL.

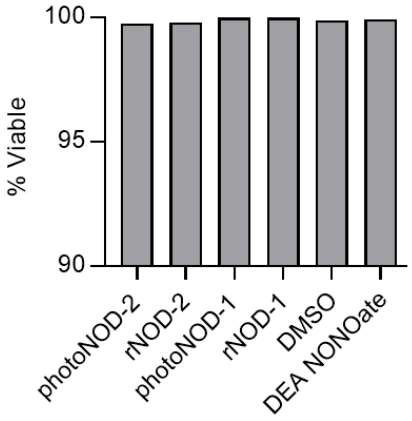

Figure S13. Percentage of viable HEK293T cells after treatment with the photoNODs and rNODs (30 μM) vs vehicle control and DEA NONOate (20 μM) after 24 h incubation in serum-containing media.

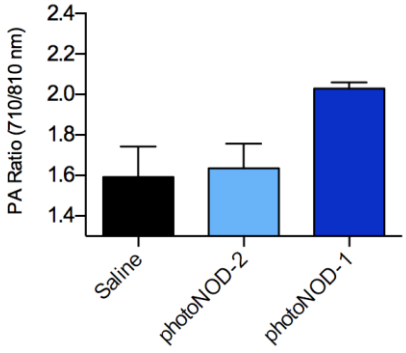

Figure S14. Ratiometric PA signal (710/810 nm) of tumor images acquired 4 hours after retroorbital administration of photoNOD-1, photoNOD-2 (1.2 mg/kg, 150 μL sterile saline with 20% DMSO) and vehicle control. Data represented as mean ± SD (n = 2).

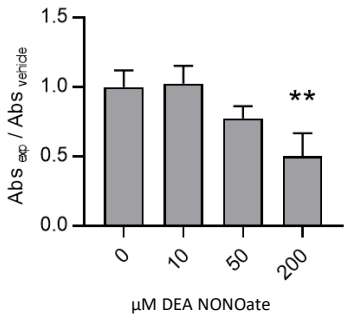

Figure S15. Proliferation of cultured 4T1 cells after incubation with DEA NONOate (10, 50, 200 μM) for 12 h relative to a vehicle control. Data represented as mean ± SD (n = 3). ** $p < 0.01$.

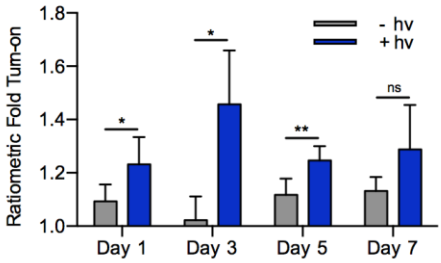

Figure S16. Ratiometric PA fold turn-on (830/700 nm) in irradiated and non-irradiated tumors of mice treated with photoNOD-1 (1.2 mg/kg, 150 μL sterile saline with 20% DMSO). PhotoNOD-1 was administered via retroorbital injection, and PA images were acquired of both tumors four hours following administration. The left tumors were then selectively irradiated for 5 minutes (700 nm), and PA images of both tumors were acquired after this period to determine ratiometric fold turn-on. Data represented as mean ± SD (n = 6). * $p < 0.05$, ** $p < 0.01$.

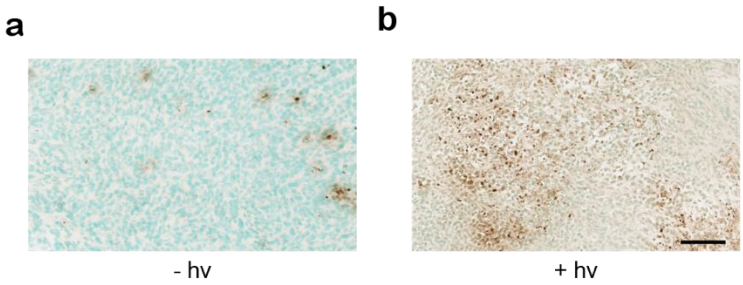

Figure S17. Histological analysis of tumor cryosections (10 μm) after treatment with photoNOD-1 with and without irradiation. Irradiation took place 4 hours following photoNOD-1 administration, and tumors were excised 15 minutes following irradiation. Cryosections were

stained with Abcam *In situ* Apoptosis Detection Kit (ab206386) according to the manufacturer's instructions and imaged using a NanoZoomer Digital Pathology System (Hamamatsu Photonics). Dark brown signal indicates positive staining for apoptosis. Scale bar represents 100 μm.

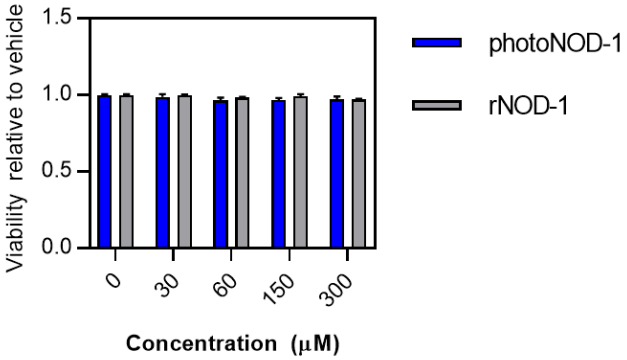

Figure S18. Cytotoxicity studies for photoNOD-1 and rNOD-1 relative to a vehicle control. 4T1 cells were incubated with dyes at 30, 60, 150, and 300 μM. Data represented as mean ± SD (n = 3).

NMR Spectra

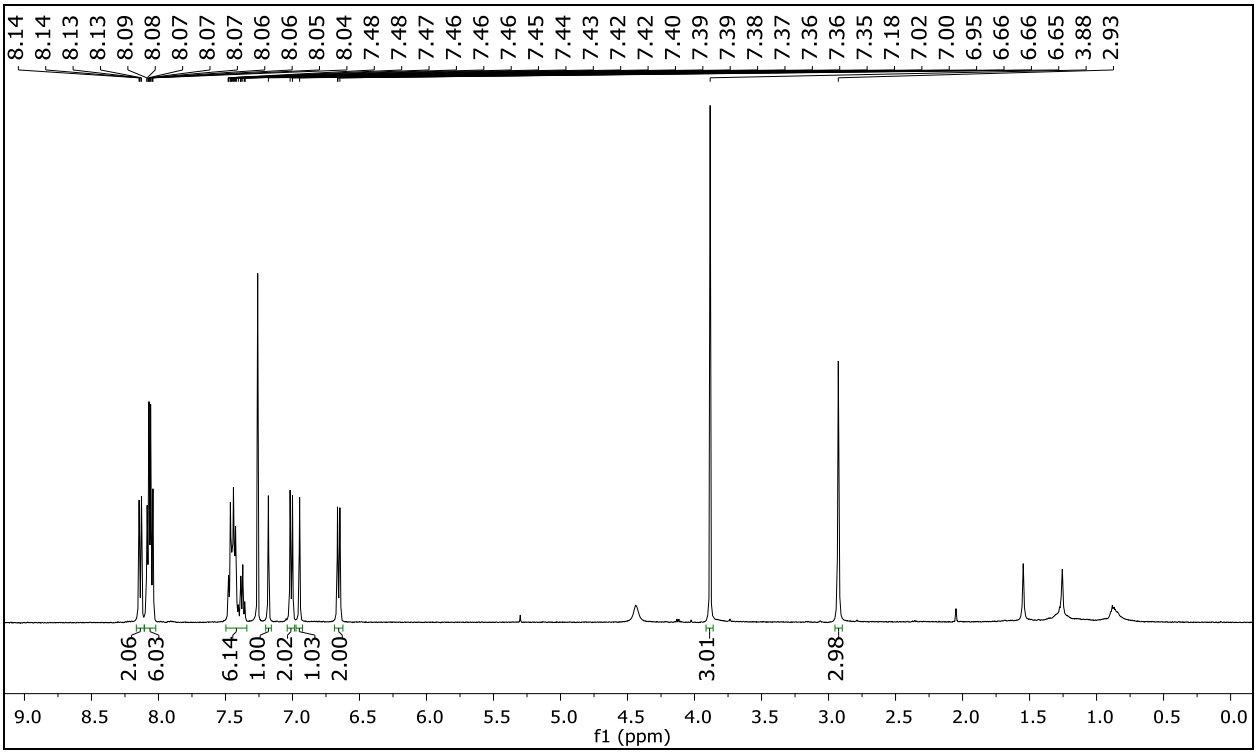

Figure S19. ^{1}H NMR of rNOD-1 ($CDCl_3$).

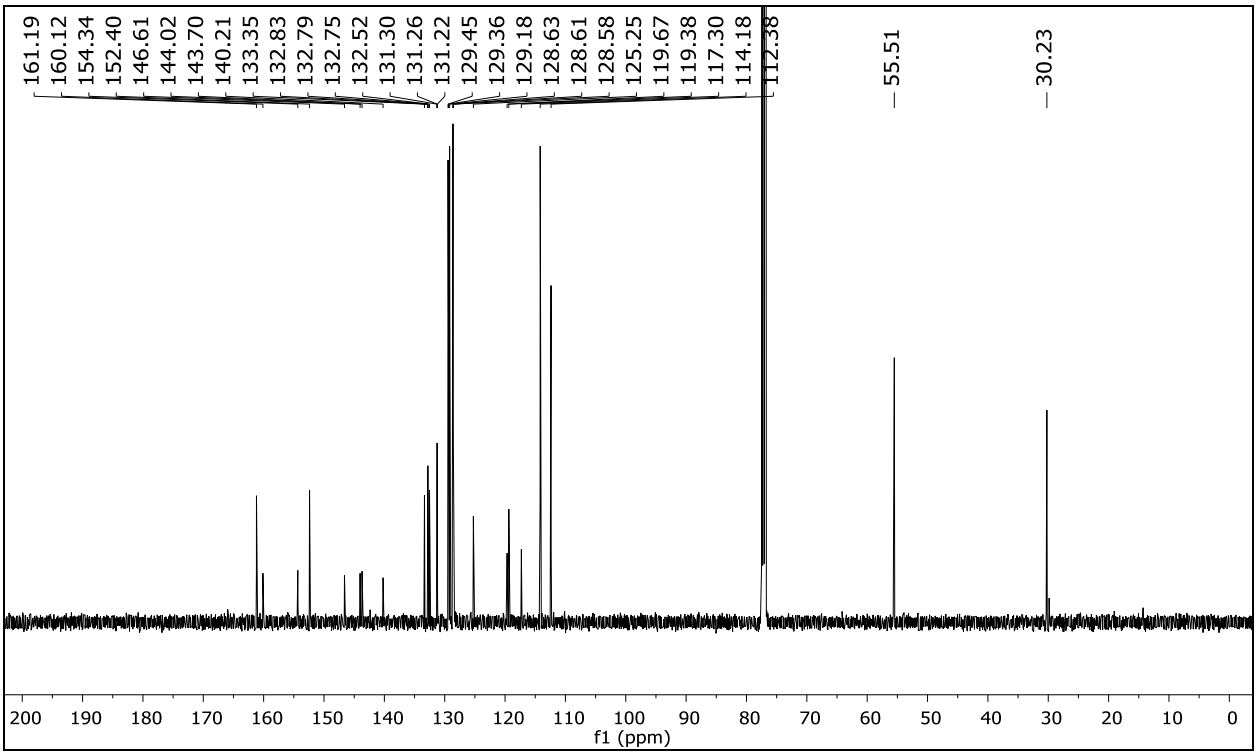

Figure S20. ^{13}C NMR of rNOD-1 ($CDCl_3$).

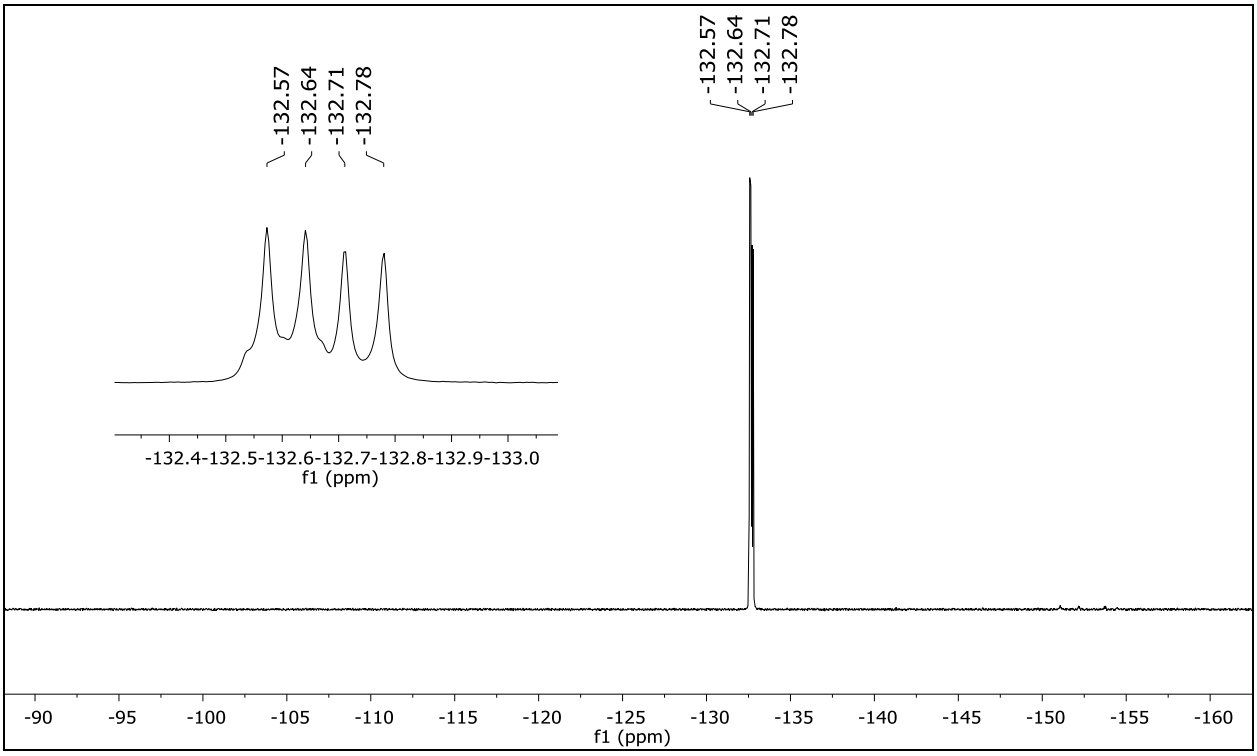

Figure S21. ^{19}F NMR of rNOD-1 ($CDCl_3$).

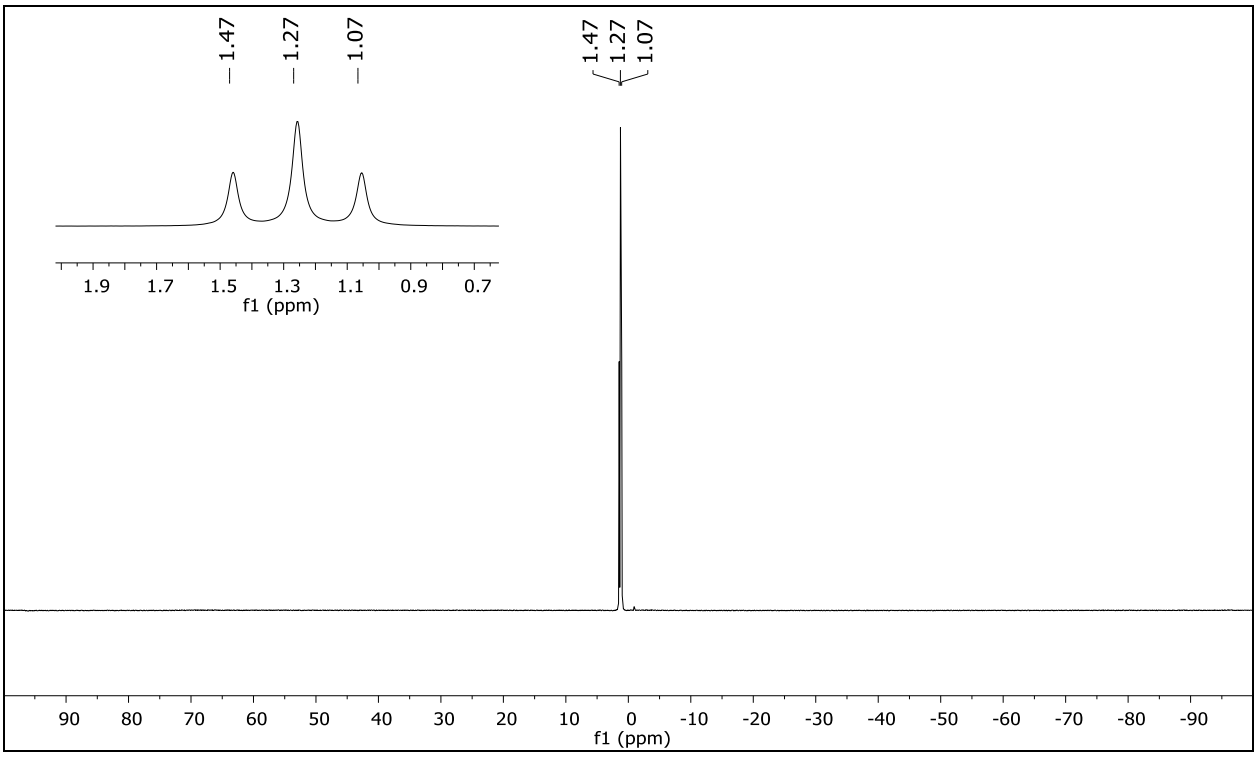

Figure S22. ^{11}B NMR of rNOD-1 ($CDCl_3$).

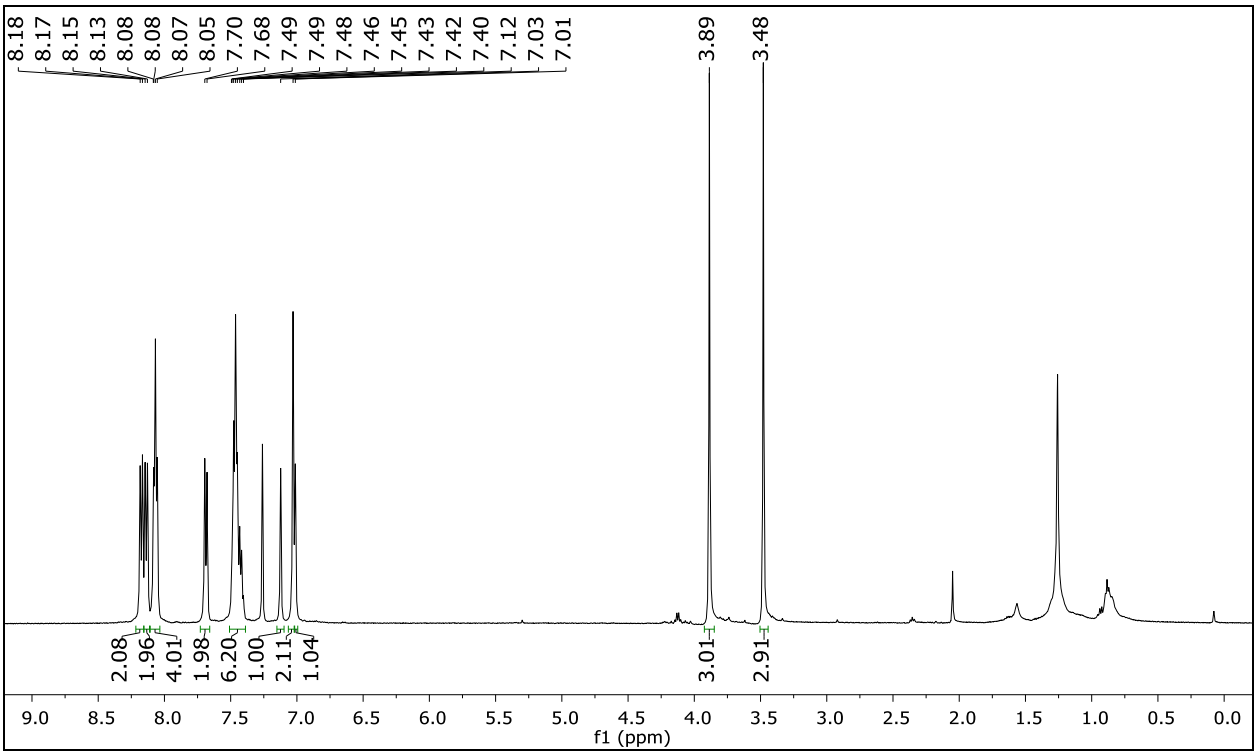

Figure S23. ^{1}H NMR of photoNOD-1 ($CDCl_3$).

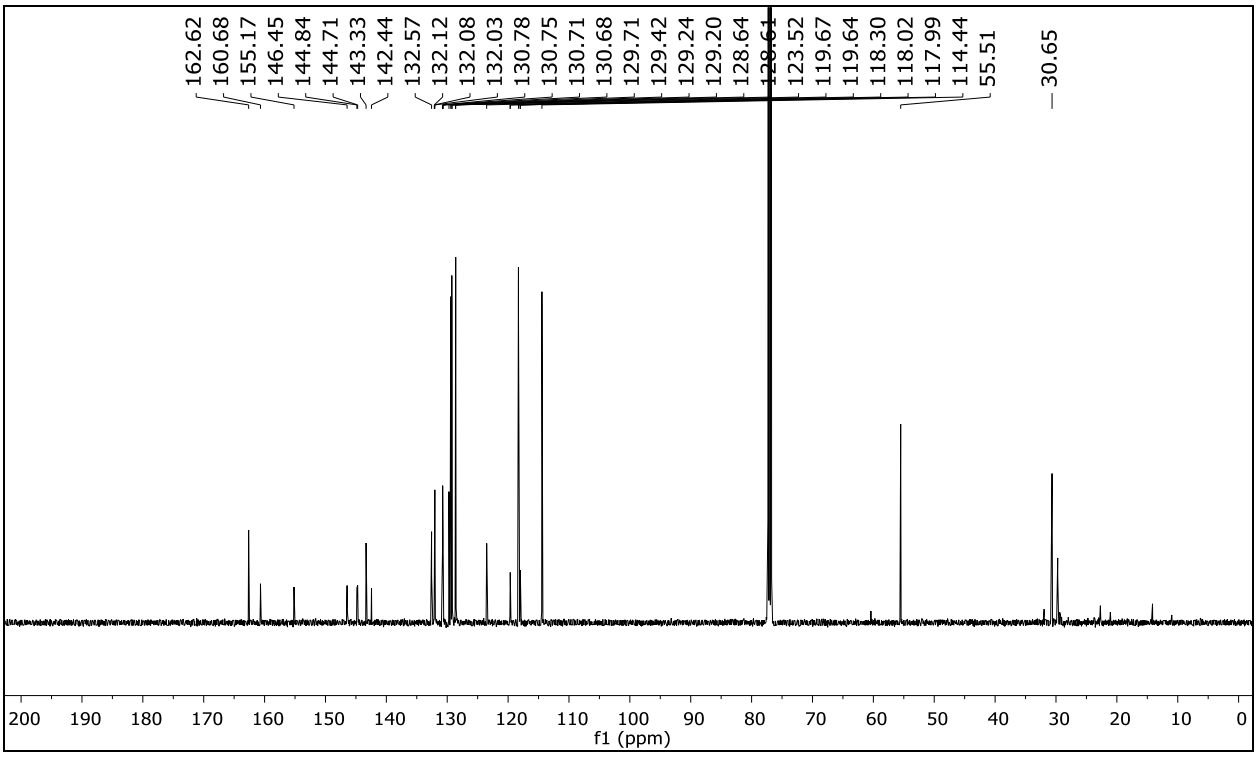

Figure S24. ^{13}C NMR of photoNOD-1 ($CDCl_3$).

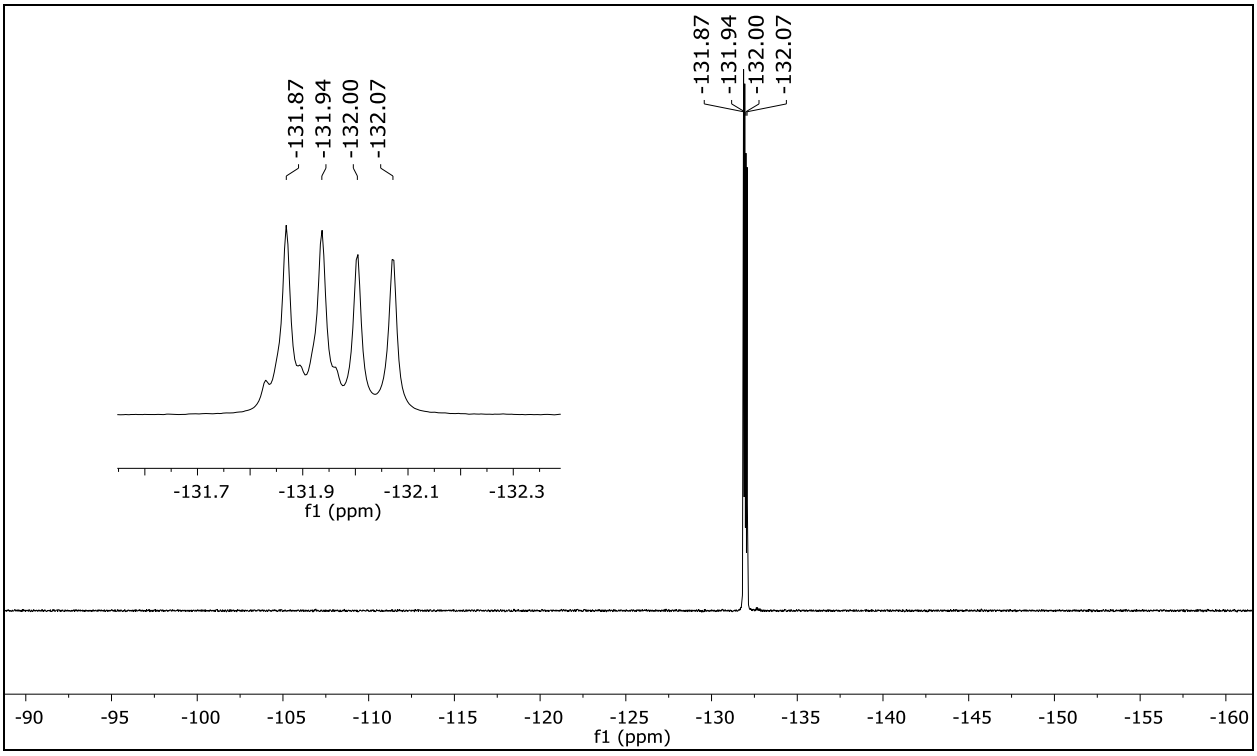

Figure S25. ^{19}F NMR of photoNOD-1 ($CDCl_3$).

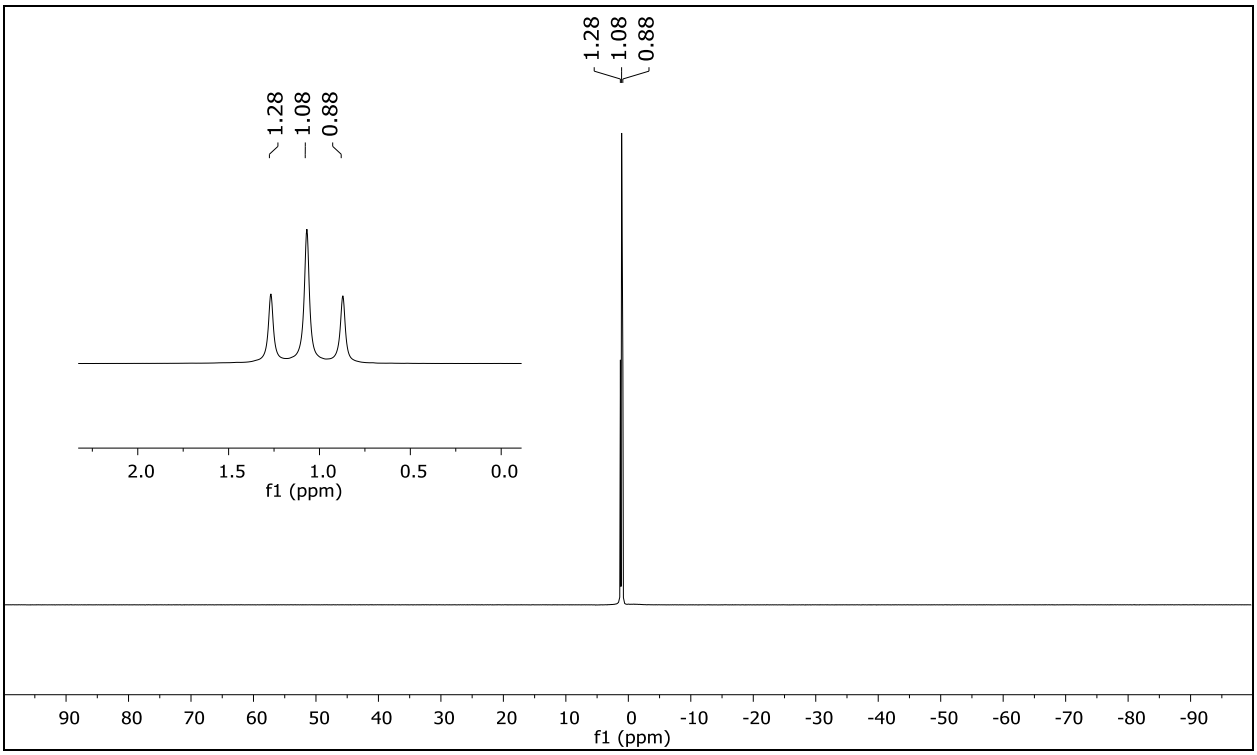

Figure S26. ^{11}B NMR of photoNOD-1 ($CDCl_3$).

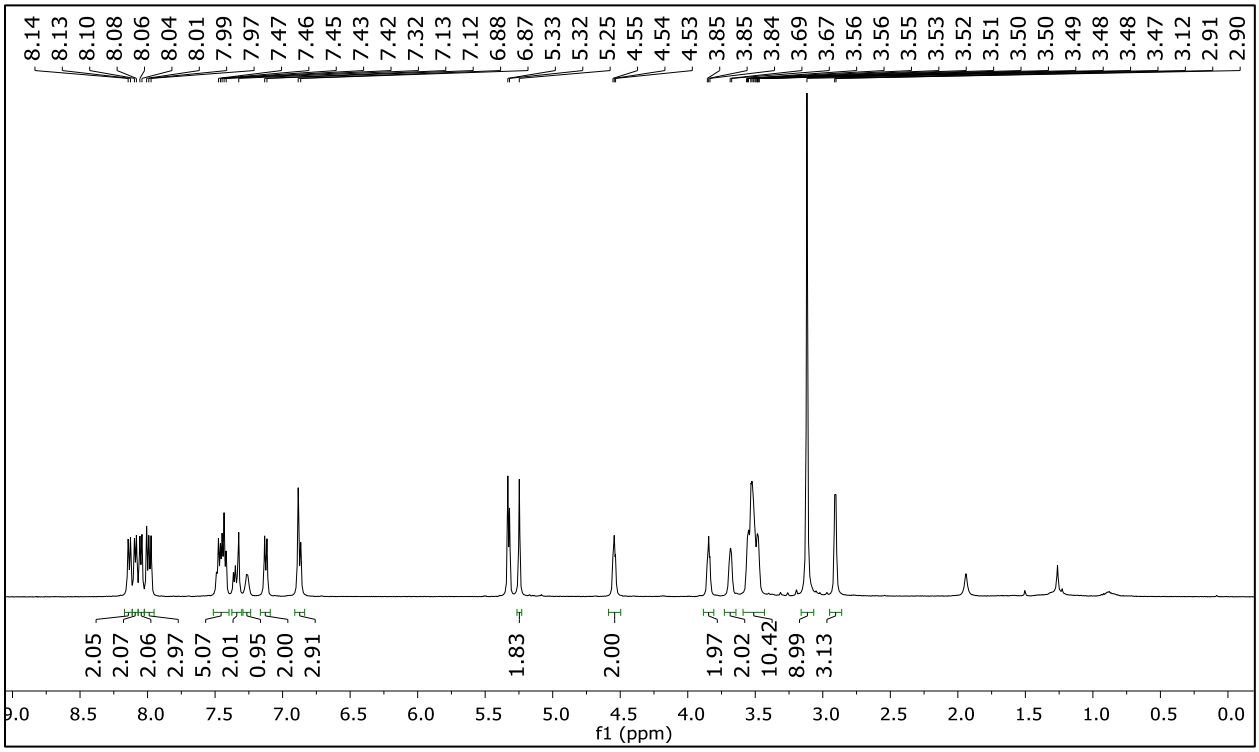

Figure S27. ^{1}H NMR of rNOD-2 (CD_2Cl_2).

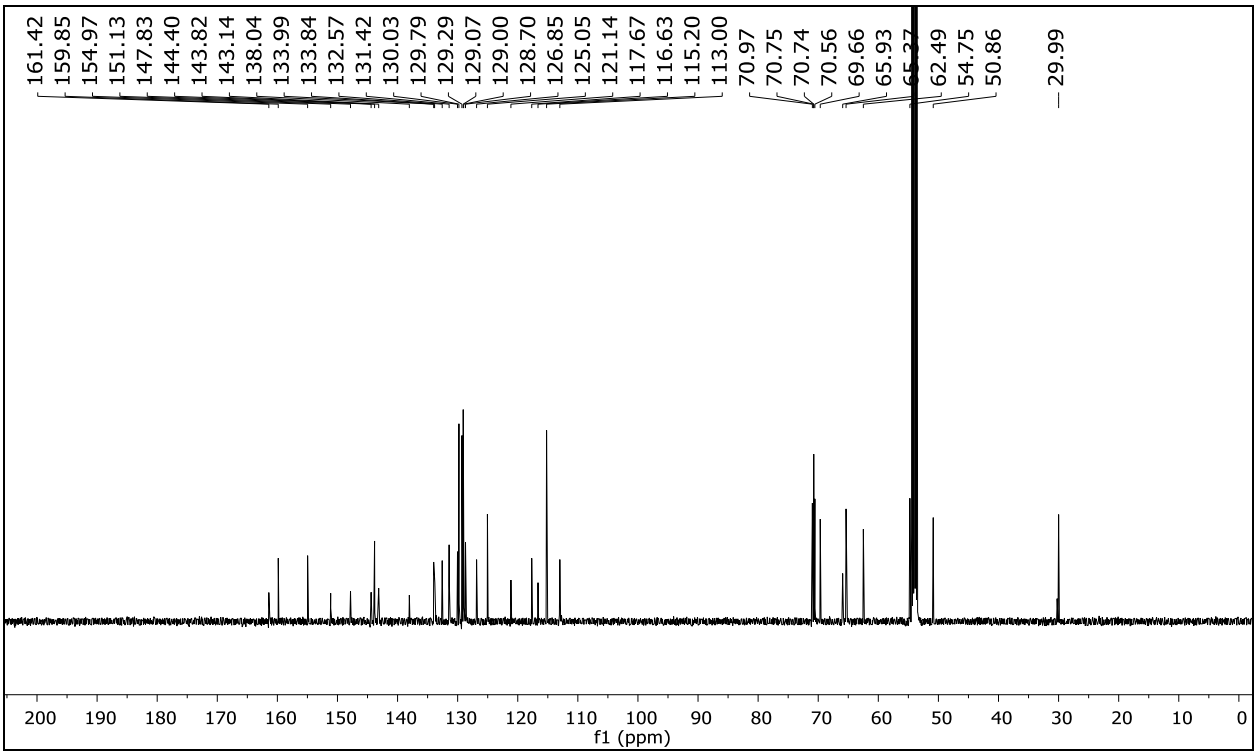

Figure S28. ^{13}C NMR of rNOD-2 (CD_2Cl_2).

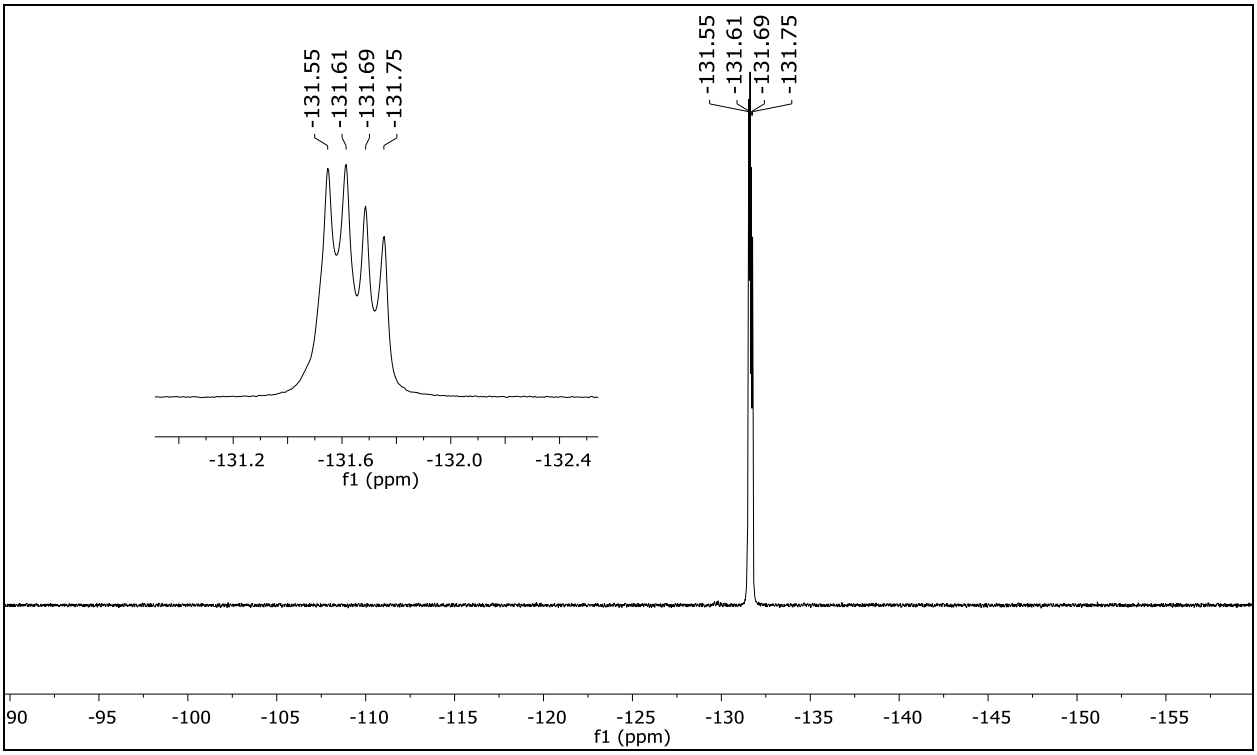

Figure S29. ^{19}F NMR of rNOD-2 (CD_2Cl_2).

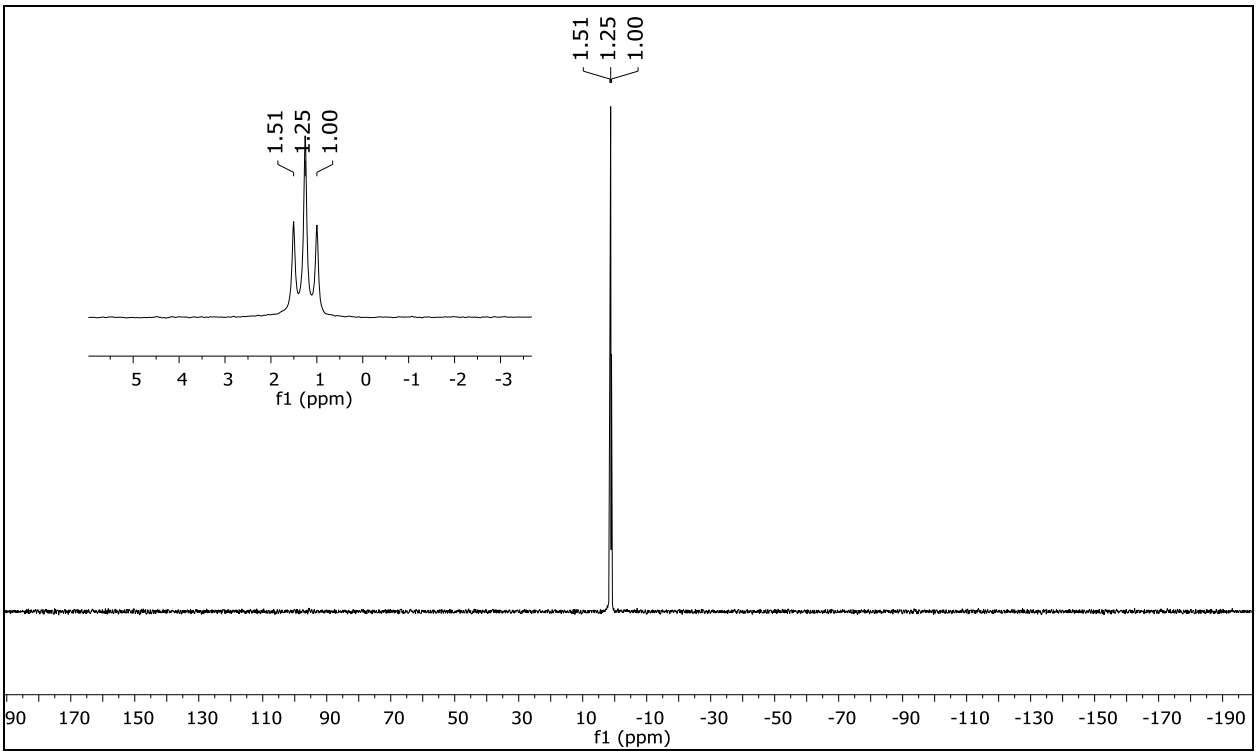

Figure S30. ^{11}B NMR of rNOD-2 (CD_2Cl_2).

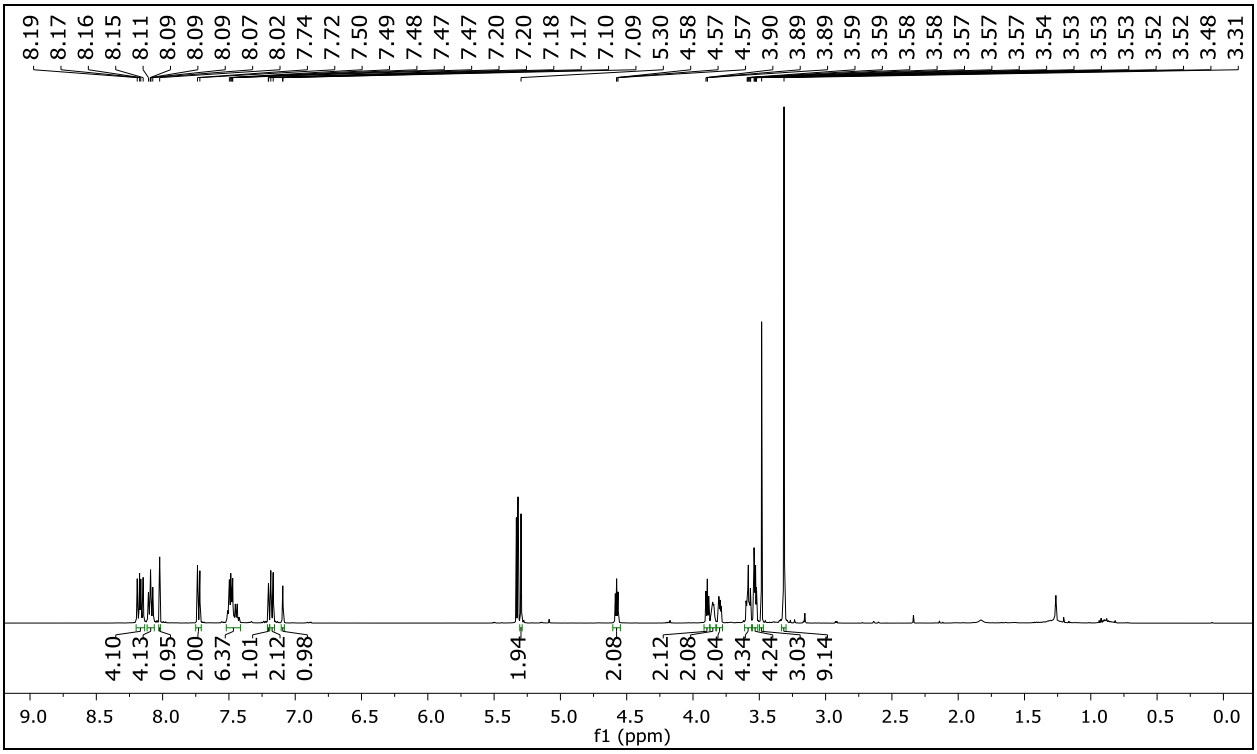

Figure S31. ^{1}H NMR of photoNOD-2 (CD_2Cl_2).

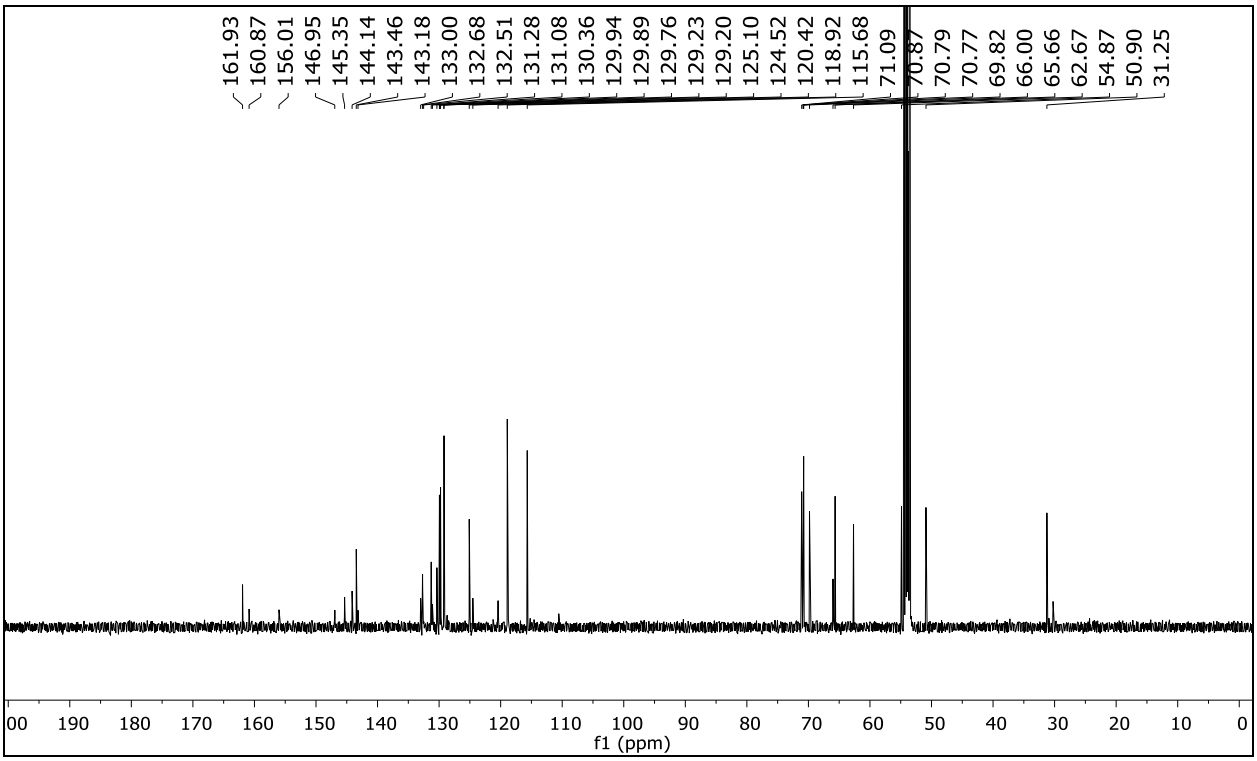

Figure S32. ^{13}C NMR of photoNOD-2 (CD_2Cl_2).

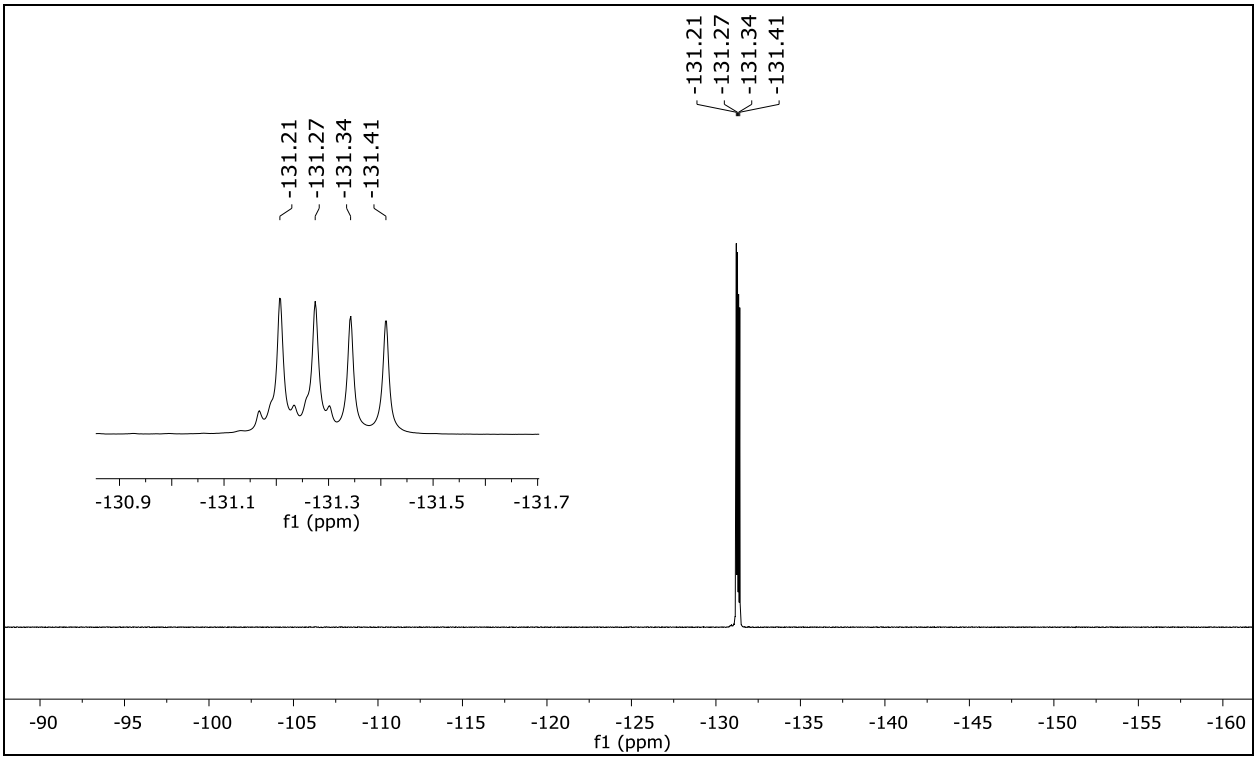

Figure S33. ^{19}F NMR of photoNOD-2 (CD_2Cl_2).

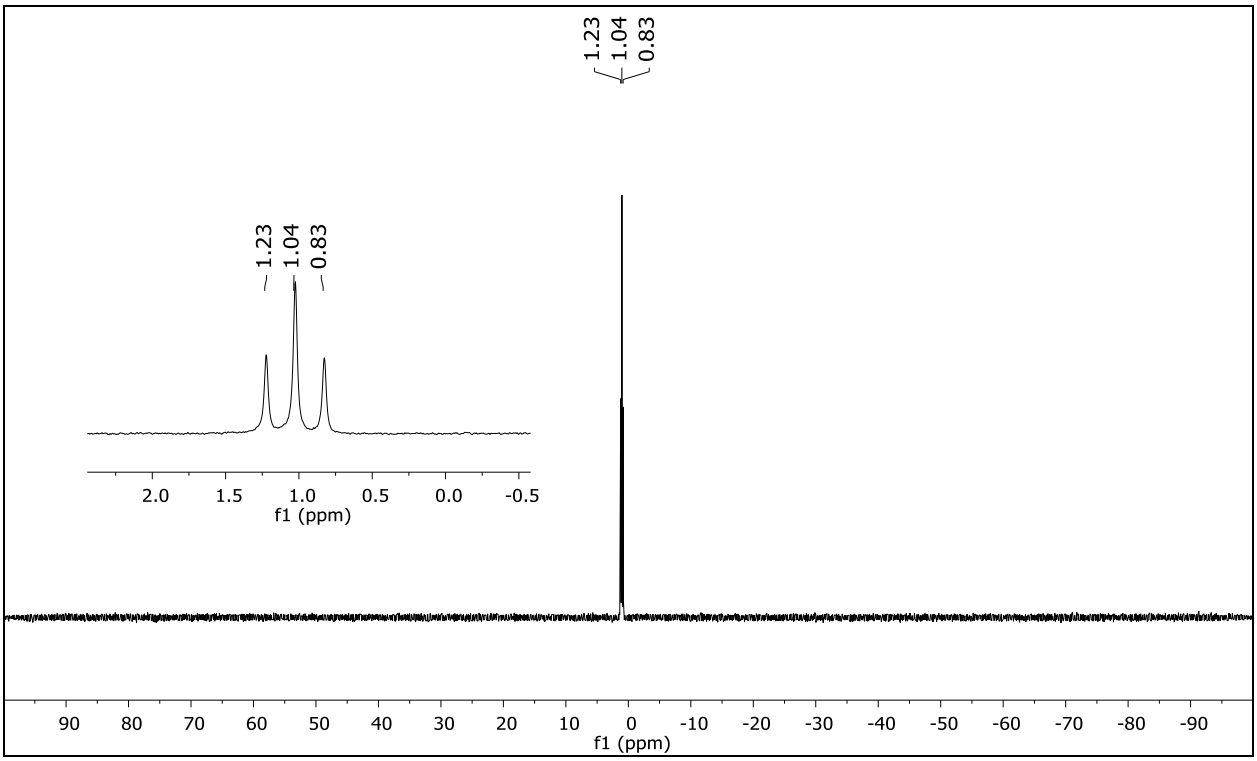

Figure S34. ^{11}B NMR of photoNOD-2 (CD_2Cl_2).

References

1. Reynolds III, J. E., Josowicz, M., Tyler, P., Vegh, R. B. & Solntsev, K. M. Spectral and redox properties of the GFP synthetic chromophores as a function of pH in buffered media. *Chem. Commun.* **49,** 7788 (2013).